ACS APPLIED BIO MATERIALS Cite This: ACS Appl. Bio Mater. 2018, 1, 1094−1101 Article www.acsabm.org

Ultracompact Nanotheranostic PEG Platform for Cancer Applications

Thomas Hopkins,[†,§] Scott D. Swanson,[‡,§] Jeremy Damon Hoff,[†] Natalie Potter,[†] Rahil Ukani,[†] and Raoul Kopelman*[,†]

[†]LSA Chemistry, University of Michigan, 930 North University Avenue, Ann Arbor, Michigan 48109, United States
[‡]Department of Radiology, University of Michigan, 1301 Chatherine Street, Ann Arbor, Michigan 48109, United States

Supporting Information

ABSTRACT: We present a new targetable nanoconstruct (NC) capable of simultaneously serving as a therapeutic platform for photodynamic therapy (PDT) as well as a magnetic resonance (MR) molecular imaging agent, free of heavy metal atoms. PDT has seen much interest with the introduction of NC-assisted cell-specific targeting of the photosensitizer (PS). The previously reported ultrasmall 8-arm polyethylene glycol amine (8PEGA) NC, with an attached chlorin e6 (Ce6) PS, yielded promising results for PDT of heart arrhythmia, *in vivo* and *ex vivo*, on live rat and sheep hearts, respectively, when using targeting peptides for *cell-specific ablation* of cardio-myocytes. Here we explore the extension of this NC-based PDT to cancer. For this purpose, we switched the targeting peptide from CTP-cys to F3-cys. Notably, the 8PEGA-Ce6 NCs have a superior reactive oxygen species (ROS) production compared to traditional Ce6 encapsulated polyacrylamide (PAAm) NCs, which should be advantageous for PDT. This NC is also cyto-compatible and offers chemical flexibility for the attachment of a choice of targeting peptides. Finally, this label-free 8PEGA NC can be directly and selectively imaged by MRI, using standard spin−echo imaging sequences with large diffusion magnetic field gradients to suppress the water signal. Notably, due to its ultrasmall size this NC is also expected to have improved *in vivo* penetration and bioelimination, as was already shown in previous biodistribution studies.

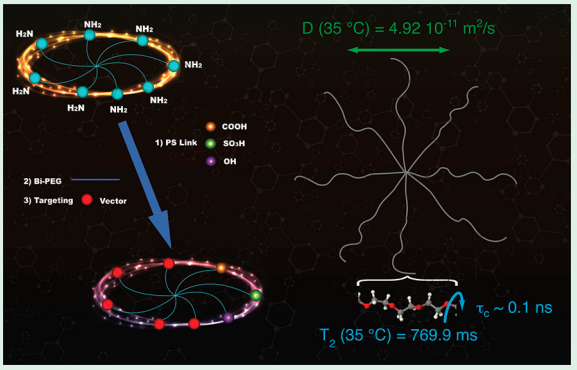

KEYWORDS: *cancer, MRI agent, nanoparticles, PDT, PEG*

INTRODUCTION

We describe here a multifunctional, ultrasmall nanoplatform that has a plethora of desirable therapeutic and diagnostic (theranostic) properties. Specifically, we demonstrate its superior photodynamic efficacy, illustrated by its application to cancer cells. We also emphasize its unique performance as an excellent, nontoxic, molecular imaging agent for MRI.

Photodynamic therapy (PDT) is a method for ablating biological tissue by photo-oxidation utilizing photosensitizer (PS) molecules. PDT has been pioneered by Dougherty et al. at the Roswell Park Cancer Institute for treatment of skin cancer and other diseases.[1,2] Since the start of the millennium, the field has received additional attention due to the emergence of *cell-targeted PDT*. Both spatial (laser focused) and biological (cell selective) selectivity is achieved by employing nanoconstructs (NCs) with targeting antibodies or peptides, which also extended PDT treatment to subsurface tumors.[2−8] In general, the use of NCs allows for protection of a PS from the bioenvironment, and *vice versa*, for bypassing the immune system[3−12]

Recently, we reported on the use of PDT for treating *heart arrhythmia* in rat and sheep models.[13] The NC utilized was the octopus-like, ultracompact, and highly biocompatible polymer, *8-arm polyethylene glycol amine* (8PEGA). The amine-terminated arms were used to anchor the algae-derived PS, chlorin e6 (Ce6), and a targeting moiety for cardio-myocytes.[13] Here, the relatively small sized (<20 nm) 8PEGA derived NCs penetrated the very dense tissue of the heart muscle, selectively accumulating in cardio-myocytes and thus allowing their photodynamic ablation under mild near-infrared illumination. Given the success of cell-selective heart arrhythmia ablation, we focus here on adapting an analogous NC for treating cancer.

In the heart arrhythmia project, the method of tagging 8PEGA with CTP (cardiac targeting peptide) for targeting was the very well understood maleimide−thiol reaction. Similarly, we expect any peptide to be viable for attachment to 8PEGA, provided it is cysteine terminated. The F3-cys peptide is a specific cancer-targeting peptide studied by our lab at great length.[8,14] It was thus chosen as our test case for extending the

Received: July 11, 2018
Accepted: September 7, 2018
Published: September 20, 2018

   DOI: 10.1021/acsabm.8b00315
ACS Appl. Bio Mater. 2018, 1, 1094−1101

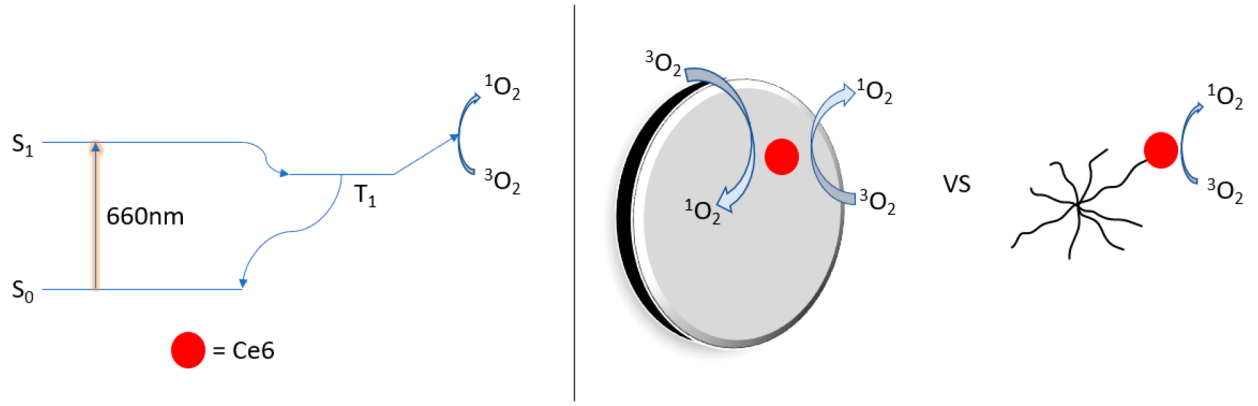

Figure 1. Difference in structural representation of Ce6 delivery and ROS production efficacy (not drawn to scale). Left: basic Jablonski diagram of how ROS is produced by Ce6. Right: Encapsulated Ce6 vs anchored to 8PEGA; difference in how ROS may move shows a clear change in efficacy.

application of 8PEGA-Ce6 from arrhythmia to cancer. HeLa 229 cells sourced from ATCC were chosen as the model system of interest due to their robust nature and known overexpression of nucleolin,[15] the specific target of the F3-cys peptide.[14] While our initial interest in 8PEGA stemmed from its small size (sufficient to penetrate heart muscles) and its biocompatibility, in this work we focus on: (1) its ability to optimize ROS production with a given PS and (2) its ability to function as a molecular imaging agent for MRI. The optimized ROS production is expected for this NC due to the direct contact of the PS Ce6 with the oxygenated environment, in contrast to when it is encapsulated inside a standard model matrix, such as in polyacrylamide hydrogel nanoparticles (PAAm NPs).[16] We demonstrate here an increased ROS production efficacy, biocompatibility, and flexibility in targeting when utilizing this NC.

The high molecular weight (40 kDa), flexible chain dynamics of the 8PEGA group, and its specific structure also create favorable conditions for highly selective molecular imaging using MRI. Specifically, the slow diffusion constant and transverse spin relaxation rate of 8PEGA combine to allow diffusion-weighted MRI sequences which suppress surrounding water and fat signals, providing a very clean image of 8PEGA. We show here that the 8PEGA MR signal is selectively detected and is proportional to its concentration. We also emphasize its biocompatibility, compared to current heavy metal atom MRI imaging agents.

RESULTS

Complete 8PEGA Characterization. We compared the ROS production of Ce6 when attached to 8PEGA vs when encapsulated in polyacrylamide (PAAm), where the two competing nanostructures are represented in Figure 1. Figure S1 contains the "*k-value*" plot of the relative ROS production of PAAm-encapsulated Ce6. The *k*-value is a measure of the kinetic rate at which ROS is produced by Ce6, as measured by the first-order decay of ADPA fluorescence. While the *k*-value of 8PEGA was determined by us before,[13] to generate *k*-values that are comparable, the OD of the PAAm-Ce6 NPs[16] was adjusted by UV/vis to the optical density (OD, 0.12) of the previously reported 8PEGA-Ce6 at 660 nm.[13] Table 1 shows the relative results for the two NCs when normalized for their literature ODs.

Table 1. *k*-Values of the Two Discussed NCs at OD = 0.12 for 660 nm

nanoplatform	OD	*k*-value
8PEGA-Ce6	0.12	2.99×10^{-04} s^{-1}
Ce6/PAAm NP	0.12	1.94×10^{-04} s^{-1}

The diameter of the NC 8PEGA is also calculated by Stokes−Einstein approximately (discussed in the MRI/NMR characterization section, Figure S2) and TEM (Figure S3).

Figure 2 shows the absorption spectrum of the F3−8PEGA-Ce6 conjugate; we find that the characteristic peaks at 660 nm are preserved, compared to the nontargeted NCs.[13] For clarity, the chemical modification of 8PEGA-Ce6 with F3-cys is shown in Scheme 1.

Dark Toxicity of HeLa Cells. Flow cytometry was employed as a method of testing the biocompatibility of this NC to test for dark toxicity. Cells were tested at a concentration of 200 μg/mL F3−8PEGA-Ce6; control cells denote a data group with no F3−8PEGA-Ce6 NCs added. As can be seen from Figure 3, no significant toxicity was observed. A concentration of 200 μg/mL was chosen for its use in previous PAA NP construct cell viability assays.[16−18]

PDT Efficacy in Vitro. As a control test to eliminate the possibility of simple cell stress from the excitation light, HeLa cells without F3−8PEGA-Ce6 were plated and illuminated for the same length of time and power as used in PDT for NC-treated cells (50 mW/cm^2, 10 min). After illumination (Figure 4A, B) there is an insignificant change in cell morphology, no change in the cytosolic stain calcein AM fluorescence counts, and no signs of membrane blebbing (a hallmark of apoptosis).

We observe a remarkable difference in the calcein AM fluorescence after photoillumination of the cells with F3−8PEGA-Ce6 (Figure 4C,D). While there was no observable propidium iodidie (PI) fluorescence prior to illumination (data not shown), after illumination cell membrane impermeable PI can be seen to stain the nuclei of the cells (Figure 4E).

The translational diffusion constant, *D*, and relaxation times T_1 and T_2 of 8PEGA were measured at 25 and 35 °C (Table 2, Figure S2). Images in solution of 8PEGA (nonmodified) were gathered to demonstrate generation of clean images when water/fat was suppressed (Figure 5) and their concentration-dependent response (Figure 6).

The response can be seen to be linear with concentration (Figure 6), consistent with images gathered with water suppression techniques (Figure 5B). Tested concentrations

DOI: 10.1021/acsabm.8b00315
ACS Appl. Bio Mater. 2018, 1, 1094−1101

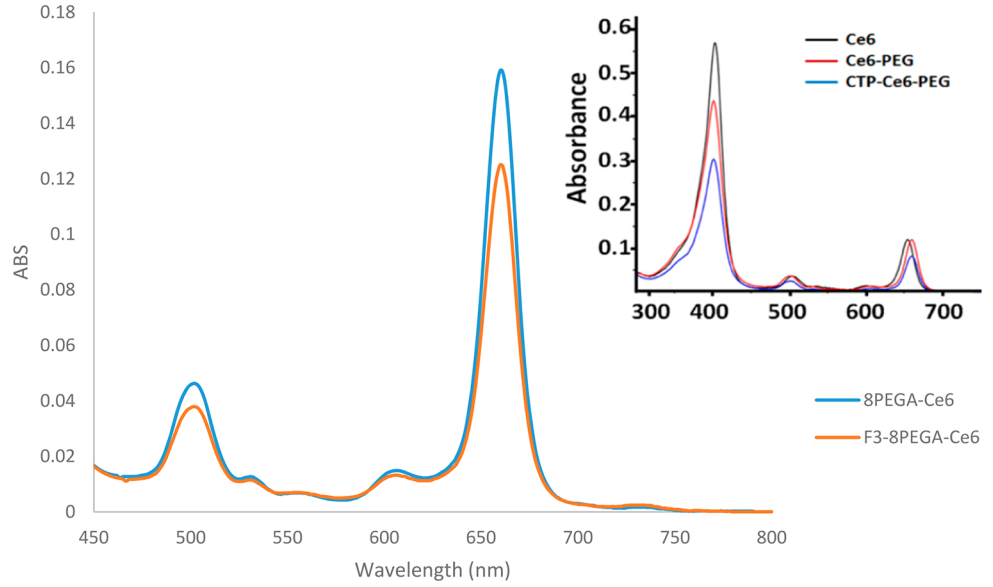

Figure 2. UV/vis spectrum of 8PEGA-Ce6 and F3−8PEGA-Ce6 in PBS at 0.1 mg/mL. Inset is of 8PEGA modification with CTP and Ce6, reproduced with permission from ref 13.

Scheme 1. Modification of 8PEGA-Ce6 with F3-Cys Peptide, As Reported in This Paper

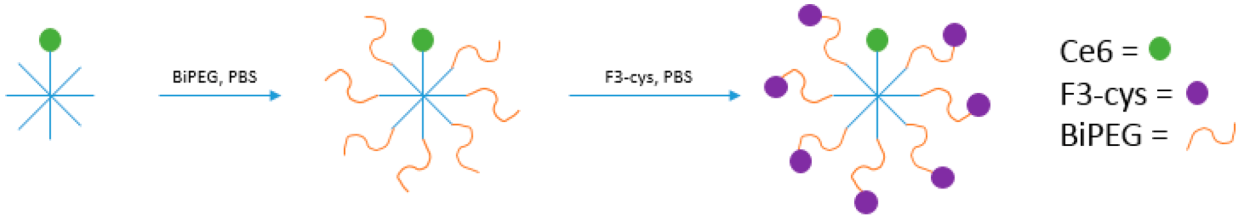

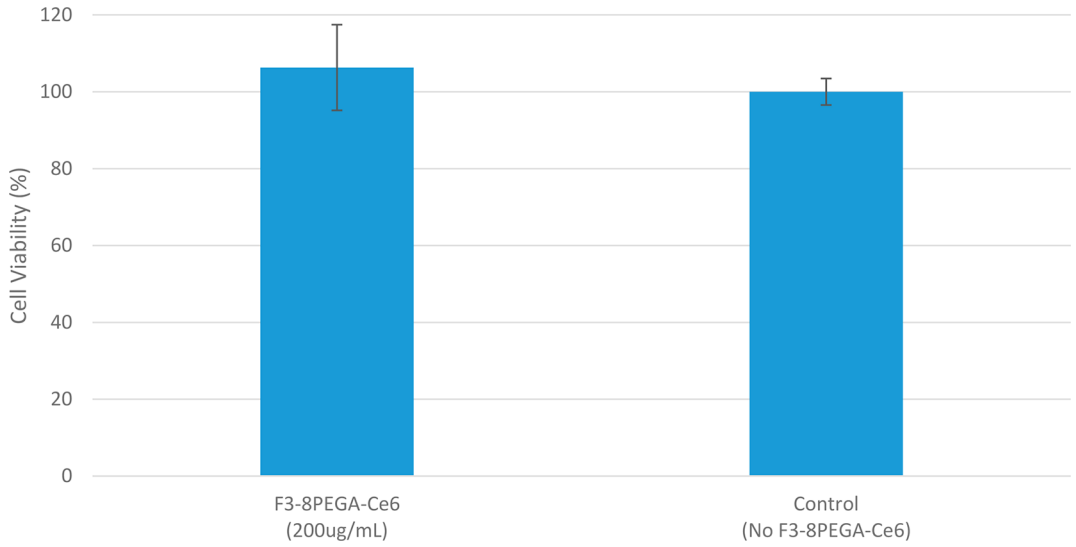

Figure 3. Hemocytometry cell population results. Incubation conditions: 200 μg/mL F3−8PEGA-Ce6 for 24 h in wells seeded with 200 000 cells (passage 30); $N = 3 \times 3$ for control and test groups (3 plates each, tested 3 times each). Control group of cells contain no F3−8PEGA-Ce6 NCs, under the same conditions. The results show near identical cell populations.

were 0, 2.38, 4.77, 9.54, and 19.08 mg/mL 8PEGA in H_2O. In addition, the Stokes−Einstein equation 1

$$r = kT/6\pi\eta D_{trans} \quad (1)$$

is employed to calculate the size of 8PEGA to verify TEM results; the diameter is calculated to be 10.96 nm at 35 °C, consistent with the ∼10−12 nm range found in the 13 measured NCs (Figure S3).

DISCUSSION

We hypothesized that Ce6−8PEGA would be a more efficient ROS producing platform, compared to hydrogel NPs, based on

DOI: 10.1021/acsabm.8b00315
ACS Appl. Bio Mater. 2018, 1, 1094−1101

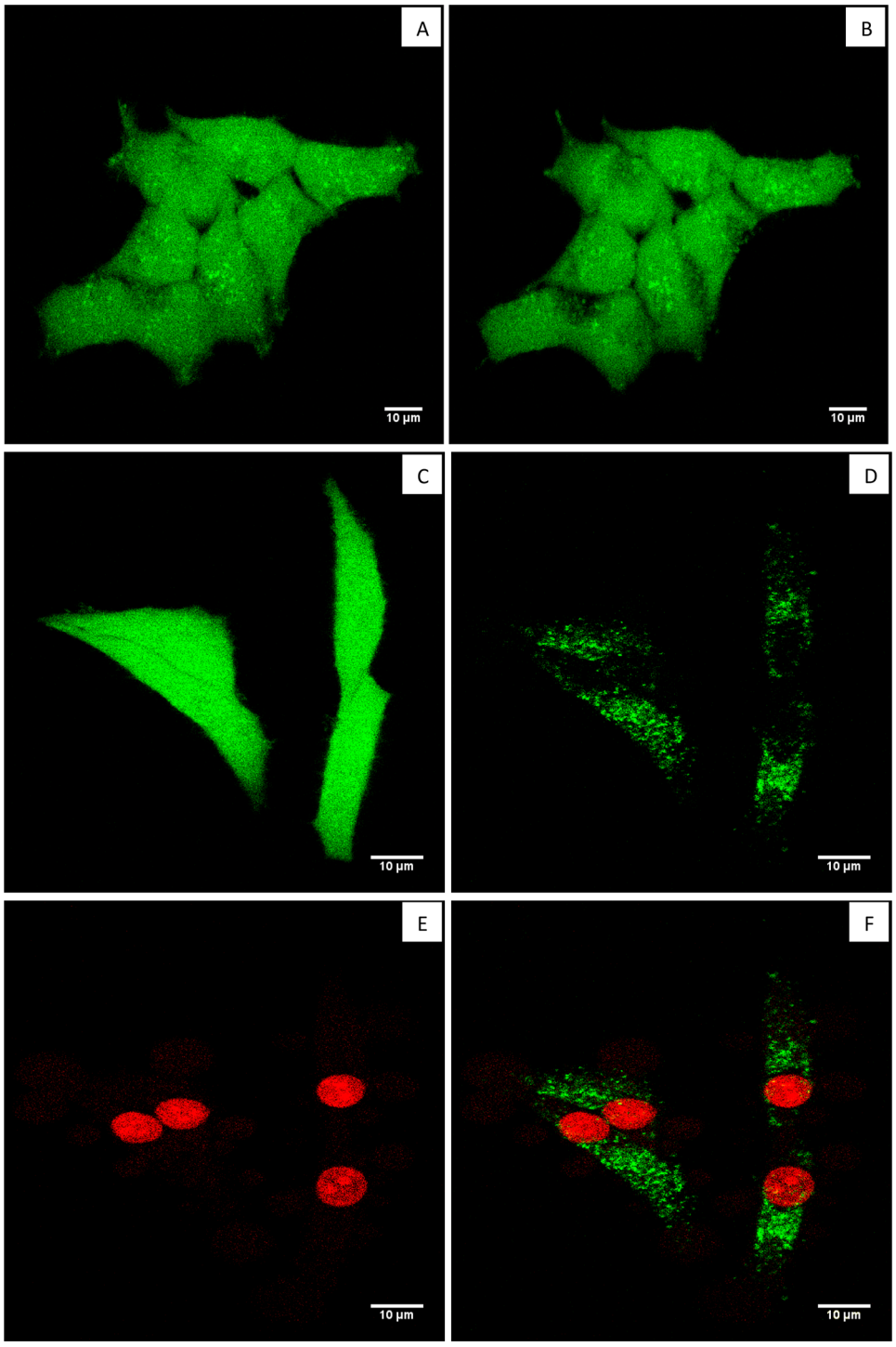

Figure 4. PDT testing images of HeLa cells. (A) Calcein AM fluorescence of PDT control cells (no F3−8PEGA-Ce6). (B) Calcein AM fluorescence of PDT control cells 2 h after illumination. (C) Calcein AM fluorescence of test cells (with F3−8PEGA-Ce6) prior to PDT. (D) Calcein AM fluorescence of test cells 2 h after PDT. (E) PI fluorescence 2 h after PDT. (F) Merge of D and E. PDT test plates were incubated with 200 μg/mL F3−8PEGA-Ce6 for 2 h prior to PDT and all cells illuminated at a total fluence of 50 mW/cm^2 for 10 min, using a 692 ± 20 nm filter and arc lamp.

Table 2. Relaxation Times and Translational Diffusion Constant of 8PEGA at 25 and 35 °C Measured at 16.4 T[a]

T (°C)	T_1 (ms)	T_2 (ms)	D (10^{-11} m^2/s)
25	791 ± 36	586 ± 24	3.572 ± 0.015
35	934 ± 72	769 ± 31	4.923 ± 0.018

[a]Sample is 5 mg/mL L8PEGA in 25/75 (V/V) H_2O/D_2O.

the understanding that in 8PEGA the Ce6 group is in direct contact with the oxygenated environment of the cells (Figure 1). Thus, oxygen does not need to diffuse into a PAAm NP matrix encapsulating the PS, and the ROS need not diffuse out nor suffer losses due to reaction with the matrix. The *k*-value test confirms this hypothesis by showing that, when adjusted to

DOI: 10.1021/acsabm.8b00315
ACS Appl. Bio Mater. 2018, 1, 1094−1101

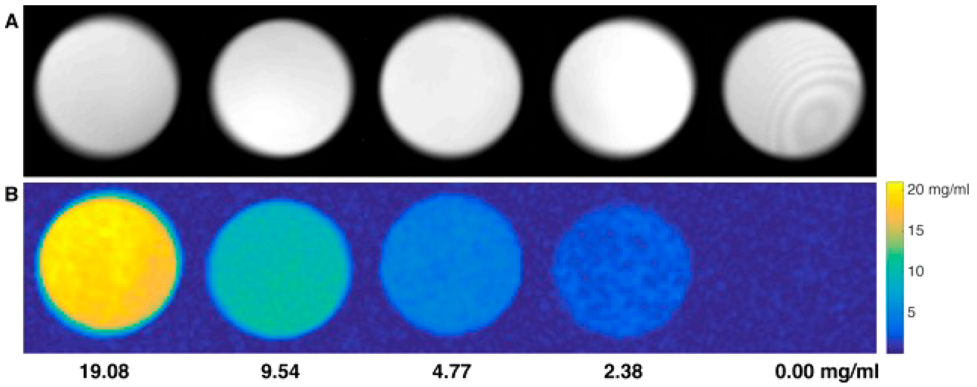

Figure 5. Diffusion-weighted spin−echo MR images of 8PEGA obtained with $b = 10^8$ s/m^2 (A) and $b = 10^{10}$ s/m^2 (B). The 110 M water proton signal dominates conventional MR images as seen in (A) but is suppressed by a factor of 10^{-10} by imaging at $b = 10^{10}$ s/m^2. The diffusion constant of 8PEGA was measured by stimulated echo pulsed field gradient NMR at 25 °C to be 3.572×10^{-11} m^2/s, allowing 70% of the initial magnetization to survive at $b = 10^{10}$ s/m^2. The color bar in (B) shows detected concentration of 8PEGA.

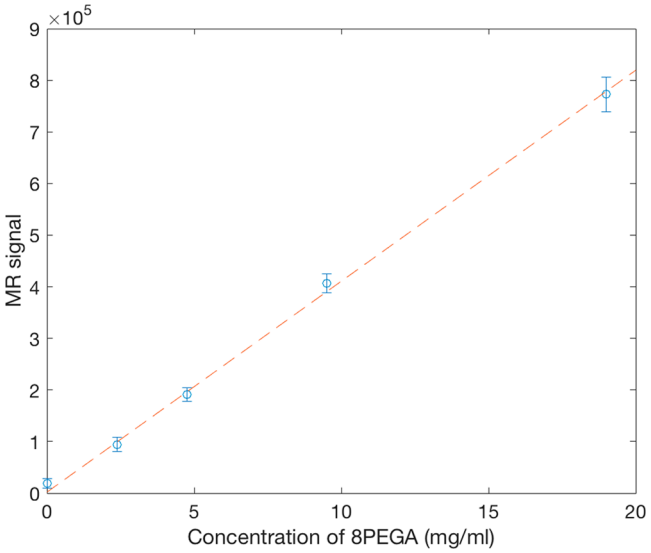

Figure 6. Concentration-dependent MRI signal of 8PEGA. A region of interest (ROI) was selected for each of the 5 vials and mean (circles) and standard deviation (error bars) of the signal computed. A linear equation was fitted to the 5 measured vials, and the result is shown as a dashed line.

identical ODs, the *k*-value of the Ce6−8PEGA[13] is about 50% larger than that of the Ce6-encapsulated PAAm NPs (Table 1).

Being that 8PEGA is a star-shaped polymer, measurement of its size by the Stokes−Einstein equation, which assumes a spherical material shape, is desirable.[19] It is found after measuring the translational diffusion coefficient, *D* (Table 2, Figure S2), that the size of polymer at 35 °C is ∼11 nm. As a secondary method of analysis, 8PEGA was stained with uranyl acetate and visualized using TEM (Figure S3). The size of the 13 chosen points is found to be approximately 10−12 nm, in good agreement with the Stokes−Einstein equation measurement.

PEGylating the surface of nanoparticles is often used as a sort of cloak and dagger approach, as PEG is largely ignored by the immune system and cells in general.[20] Here the platform itself is made of PEG only. Thus, a targeting vector is helpful not only for *in vivo* applications but also to accelerate cell uptake *in vitro*. For cancer targeting, the nucleolin targeted peptide F3-cys has been shown to be quite useful and was thus chosen for grafting onto the 8PEGA-Ce6.[18,21−23] Notably, after attachment of F3-cys, the Ce6 spectroscopic features are largely unaffected (Figure 2), indicating the preservation of photophysical properties when switching peptides (from CTP for targeting heart myocytes to F3 for targeting cancer cells).[13−15] A mild decrease in Ce6 absorption is noted for 0.1 mg/mL when compared to before and after modification but is expected, as the BiPEG and F3-cys will increase the MW of the NC.

An important aspect of this NC is its biocompatibility. The total construction is comprised of PEG, Ce6, and the homing peptide F3-cys. PEG is commonly known as a highly biocompatible substance, and F3-cys has been used as a targeting agent in our lab and others with no toxic effects *in vitro* or *in vivo*.[18,21−23] The algae-derived Ce6 has been used extensively in the literature as a PDT agent.[24−28] As such, it is expected that the combination of these three moieties should present no significant biocompatibility issues. This is confirmed *in vitro* by our hemocytometry results (Figure 3).

Before initiating PDT tests with F3−8PEGA-Ce6, the chosen laser conditions (50 mW/cm^2 for 10 min) were tested to ensure that the illumination was not a source of significant cell stress. Calcein AM images of the cells before (Figure 4A) and after (Figure 4B) illumination demonstrated little change in morphology and no signs of apoptosis. Therefore, the photoillumination source does not impart significant stress upon the cells. PDT was then initiated on 4 HeLa cells in the presence of F3−8PEGA-Ce6 at a concentration of 200 μg/mL (Figures 4C, D, E, and F). There is a significant decrease of calcein AM fluorescence after PDT in the 4 cells, indicating a loss of cytosolic contents, an event that would only occur under conditions where the cell membrane has been ruptured. Rupturing of the membrane was shown by the staining of the 4 HeLa cell nuclei with the cell-impermeable dye PI (Figure 4E); all 4 HeLa cells are dead (100% cell kill). Taking the PDT test results in conjunction with the cyto-compatibility in Figure 3, it is evident that the death of the cells is PDT-mediated.

In addition to the more efficient PDT (50% larger *k*-value), we believe that the use of 8PEGA NPs may present two more advantages: (1) The small size of the NC offers the possibility of quick renal clearance from the body,[13] a feature not afforded by larger NPs, and (2) the ability to penetrate tumor areas that have not yet undergone angiogenesis, in contrast to traditional

DOI: 10.1021/acsabm.8b00315
ACS Appl. Bio Mater. 2018, 1, 1094−1101

larger NPs that require a porous/leaky vasculature so as to be able to penetrate the tumor.[29]

Previous work has shown that ^{13}C-tagged PEG could be selectively imaged *in vivo* using heteronuclear MR methods.[30] We report here that the intrinsic flexibility of the poly(ethylene oxide) chain[31] and the slow translational diffusion of 8PEGA create an exploitable set of physical and dynamic conditions for selective MR imaging of 8PEGA protons using ^{1}H NMR. Specifically, 8PEGA's fast chain motions with correlation times of approximately 0.1 ns[31] provide sufficient averaging of the proton dipole−dipole interaction to yield a long nuclear spin transverse relaxation time T_2, measured here to be 586 and 769 ms at 25 and 35 °C, respectively. In contrast to fast internal chain dynamics, the molecule's high molecular weight yields a translational diffusion constant that is 2 orders of magnitude slower than that of water molecules. Therefore, the water signal can be effectively suppressed by large diffusion gradients[32] so that only the ethylene oxide signal will remain due to the combination of its long T_2 time and slow diffusion of 8PEGA. Notably, the MR signal intensity decays as eq 2

$$M_{xy}(b, \mathrm{TE}) = M_{xy}(0)\mathrm{e}^{-bD}\mathrm{e}^{-\mathrm{TE}/T_2} \quad (2)$$

where the b value is determined by the magnetic field gradient magnitude and duration; D is the translational diffusion constant of either water or 8PEGA; TE is the echo time; and T_2 is the transverse spin relaxation time. In addition, the symmetry of the ethylene oxide monomer gives rise to a single chemical shift for all four protons, and each 40 kDa polymer molecule carries approximately 3600 protons, creating a large molar amplification of the NMR or MRI signal. By performing a diffusion-weighted, spin−echo MR imaging experiment with high b values and long TE times, water signals, due to fast diffusion, and fat signals, due to short T_2 times, are effectively suppressed, and the 8PEGA signal is selectively imaged. *In vivo*, some signals at high b values will remain due to restricted diffusion in cells, but these signals can either be removed or distinguished from the 8PEGA signal due to the ∼1 ppm difference between water and ethylene glycol protons in traditional ^{1}HNMR.

The results (Figure 5A and B) indeed show that 8PEGA functions very well as an MR imaging agent when coupled with the above-mentioned suppression techniques. This may potentially replace other MRI contrast agents like gadolinium salts or chelates, which present health risks to certain patient groups. There is a clear difference in images without (Figure 5A) and with (Figure 5B) applied suppression techniques. The 8PEGA imaging signal is also linear with its concentration (Figure 6). Notably, when the above techniques are applied, clean and well-defined images of 8PEGA are recovered, showing clearly its viability as a potential imaging agent *in vivo*. If properly calibrated for, this would allow for quantification of the 8PEGA in biological tissue (e.g., tumor area vs filtration organs).

CONCLUSIONS

The Ce6−8PEGA NCs have been shown to be ultrasmall and possess superior ROS production, compared to encapsulated PAAm-Ce6 NPs. The successful exchange of the targeting peptides, from CTP to F3-cys, demonstrates this NC's chemical flexibility in changing targets. The F3−8PEGA-Ce6 NCs also displayed good biocompatibility *in vitro*, and their constituent composition (PEG, Ce6, F3) makes us believe that this will remain true *in vivo*. 8PEGA additionally demonstrated clear promise as a molecular imaging agent in MRI when coupled with techniques meant to suppress water and fat signals. Overall the F3−8PEGA-Ce6 presents an attractive universal NC for theranostics (imagining and PDT), from heart arrhythmia to cancer, and possibly to other pathologies. The potential benefits of rapid renal clearance and of accumulation in early stage tumors, even before angiogenesis, coupled with the MRI results, encourage a translation to animal studies. Models, protocols, and animals are currently being evaluated in further studies.

MATERIALS AND METHODS

Materials. Chlorin e6 (Ce6) and 1-ethyl-3-(3-(dimethylamino)-propyl)carbodiimide (EDC) are sourced from Frontier Scientific. 8PEGA (40 kDa) and Bi-PEG (Maleimide-PEG-Succinimydal Ester, 2kDA) is sourced from Creative PEG Works. F3-Cys peptide (KDEPQRRSARLSAKPAPPKPEPKPKKAPAKKC) is sourced from SynBioSci. 190 proof natured ethanol from Decon Laboratories. 10 kDa and 300 kDa filters for Amicon Cells and 10 kDa centrifugal filters are sourced from Amicon. DMEM [(+)-glutamine, sugar, sodium pyruvate), penicillin streptomycin, and fetal bovine serum are sourced from Life Technologies. All other chemicals are sourced from Sigma-Aldrich: acrylamide, 3-(acryloyloxy)-2-hydroxypropyl methacrylate (AHM), aminopropyl methylacrylamide hydrogen chloride salt (APMA), *N*-hydroxy succinimide (NHS), *N*,*N*′-dicyclohexylcarbodiimide (DCC), Brij L4, dioctyl sulfosuccinate sodium salt (AOT), dimethyl sulfoxide (DMSO), dimethylformamide (DMF), ammonium persulfate (APS), tetramethyl ethylene diamine (TEMED), phosphate buffer saline (0.01M, PBS), hexanes, cysteine, anthracene dipropionic acid (ADPA), calcein AM, propidium iodide (PI). HeLa 229 cells are provided by ATCC.

8PEGA-Ce6 Conjugate. Ce6 was conjugated to 8PEGA via DCC/NHS coupling in DMF.[13] Briefly, 448 μL of Ce6 solution (20 mg/mL, DMF) was activated with 154.8 μL of DCC and 172.8 μL of NHS under stirring (20 mg/mL, DMF) for 30 min. 500 mg of 8PEGA was solvated in DMF at a concentration of 50 mg/mL using sonication. Upon solvation, the Ce6 solution was added to the 8PEGA solution and allowed to stir overnight. The following day, unconjugated Ce6 was removed using 50% ethanol/PBS mixture in an Amicon Cell filtration system using a 10 kDa membrane. After purification, the solvent was exchanged with Millipore ultrapure water, and the materials were filtered using a 0.45 μm syringe filter and freeze-dried for storage.

F3−8PEGA-Ce6 Conjugate. 8PEGA-Ce6 was modified with F3 via the same methods reported by our lab over the years.[14,17,18,21−23] After modification with F3-cys, the UV/vis was then taken to ensure that the Ce6 had not aggregated in the process. Briefly, 20 mg of Bi-PEG is added to 1 mL of 8PEGA-Ce6 (20 mg/mL, PBS) and stirred for 30 min. The solution was then washed 4 × 15 minutes in PBS using a 10 kDa centrifugal filter. The resulting solution was concentrated to 20 mg/mL (by original mass), and 22 mg of F3-cys was added (220 μL, 11 mg/110 μL DMSO) and left to stir overnight. The next day, excess of cysteine was added and stirred for 2 h to cap any unreacted maleimide groups. The solution was then filtered again using a 10 kDa centrifugal filter and Millipore ultrapure water and freeze-dried for storage.

Ce6-Encapsulated Polyacrylamide Nanoparticles (PAAm NPs). Ce6 was encapsulated in PAA NPs through a slightly modified previously reported method.[16] Briefly, 5 mg of Ce6 was added to 930 μL of PBS and 100 μL of DMSO with 28 mg of APMA, 19 mg of NHS, and 16 mg of EDC. The solution is stirred at 37 °C for 2 h. Acrylamide and AHM were then added to the solution (368 mg and 52.6 μL, respectively) and sonicated to create a uniform solution. This solution was added to a 100 mL round-bottom flask containing 31 mL of hexane, 2.2 mL of Brij L4, and 1.07 g of AOT under stirring. The stirring was adjusted to where the generated vortex is just barely touching the stir bar (∼500 rpm). The contents of the flask were then

DOI: 10.1021/acsabm.8b00315
ACS Appl. Bio Mater. 2018, 1, 1094−1101

purged with nitrogen for 15 min. Nitrogen flow was removed from contact with the flask contents and maintained inside the flask. 15 mg of APS in 100 μL of water was added dropwise to initiate polymerization, and 100 μL of TEMED was added dropwise to catalyze the process. Polymerization was allowed to proceed for 2 h. Hexanes are then removed via rotary evaporation. The resulting contents were redispersed in ethanol and cleaned using 10 × 150 mL of ethanol and 5 × 150 mL of Millipore ultrapure water in an Amicon Cell using a 300 kDa filter. The purified materials are syringe filtered using a 0.45 μm filter and freeze-dried for storage.

Equipment. A Shimadzu UV-1601 UV/visible spectrophotometer was used for recording and adjusting the optical density (OD) of PAAm-Ce6 NPs. All fluorescence spectra were taken using a Fluoromax-3.

Size Analysis. The size of 8PEGA was characterized through two methods: TEM and NMR. To gather images of 8PEGA in its hydrated form, the compound was deposited on a copper grid, stained with uranyl acetate, and placed into the chamber while the grid was still wet. This enabled reasonable visualization of the low electronically dense 8PEGA by using surface tension to maintain its conformation. Size was analyzed via NMR using the Stokes−Einstein equation for translational motion (see MRI section for NMR measurements).

MRI. NMR relaxation times T_1, T_2 and translational diffusion constant, D, of 8PEGA were determined at 25 and 35 °C with a Varian/Agilent 16.4T NMR high-resolution spectrometer equipped with pulsed field gradients. T_1, T_2 and diffusion data were collected with inversion−recovery, spin−echo, and stimulated-echo pulse sequences, respectively.

T_1 times were estimated by fitting recovery of longitudinal magnetization to $M_z(t) = M_0\left(1 - 2\exp\left(-\frac{t}{T_1}\right)\right)$ where t was the time between the inversion RF pulse and sampling RF pulse. T_2 times were estimated by fitted decay of transverse magnetization to $M_{xy}(t) = M_{xy}(0)\exp\left(-\frac{t}{T_2}\right)$ where t was the time for formation of the spin echo. The translation diffusion constant D was estimated by fitting the decay of magnetization due to a pair of pulsed magnetic field gradients in a stimulated echo experiment to $M_{xy}(b) = M_0 \exp(-bD)$ where b was given by $b(G_z, \delta, \Delta) = (\gamma G_z \delta)^2\left(\Delta - \frac{\delta}{3}\right)$ where G_z is the amplitude of the applied gradient, γ the proton gyromagnetic ratio, δ the duration of the applied gradient, and Δ the time separation between the gradient pair.

Relaxation times and diffusion constant were estimated by fitting appropriate exponential functions to the NMR data using scripts written in Matlab (The Mathworks, Natick, MA). MRI was performed with a Varian/Agilent 7T animal imaging system using a 120 mm diameter shielded gradient set capable of 400 mT/m and a 40 mm millipede RF coil. The images were created with a diffusion-weighted, spin−echo sequence with TR/TE of 500/200 ms and b values of 10^8 and 10^{10} s/m^2 for Figures 6A and 6B, respectively.

Reactive Oxygen Species (ROS) Evaluation. We use the so-called "k-value" test, a method of relatively quantifying the amount of ROS produced (larger k-value = more ROS).[11] The 8PEGA-Ce6 ROS k-value was previously reported at an OD of 0.12 at 661 nm.[13] To establish comparable k-values, the PAAm-Ce6 NPs are normalized to the OD of 8PEGA-Ce6 reported data (adjusted to OD = 0.12 at 660 nm) and the k-value evaluated via the same means as previously reported.[11,13] Briefly, 80 uL of ADPA (0.3 mg/mL) was added to 2 mL of OD = 0.12 PAAm-Ce6 NPs in PBS. The fluorescence of ADPA is taken before illumination with 661 nm light and recorded at 427 nm; this was repeated after every 300 s with 661 nm illumination. The ADPA 427 nm data points were then plotted as $\ln(I/I_0)$ vs time, where the slope is the resulting k-value.

Cell Culture PDT Test. HeLa cells were chosen as the cancer cell test line due to their robust nature. These cells were grown using DMEM culture medium containing 1% PenStrep and 10% fetal bovine serum. The cells were at passage 30 when used. An arc lamp was used as the excitation source for PDT and control tests. Briefly, a 35 mm culture dish was seeded with 100 000 cells and incubated with 200 μg/mL of F3−8PEGA-Ce6 for 2 h. For the cell live/dead tests the cells were stained using calcein AM green. After incubation, the cells were washed 3 times with prewarmed Dulbecco's PBS (DPBS), and 1 mL of prewarmed colorless DMEM (no serum) is added. A 20 uL solution of propidium iodide (1 mg/mL) was added as a necrotic cell death indicator for evaluating the PDT.

Confocal Imaging. Confocal imaging was performed using an ISS ALBA time-resolved confocal microscope, with an IX-81 Olympus microscope body and a U-Plan S-APO 60X 1.2NA water immersion objective. A Fianium supercontinuum laser with an acousto-optical filter was used to generate picosecond-excitation pulses at a wavelength of 488 nm at a repetition rate of 20 MHz. Fluorescent emission was separated into two channels by a 592 nm short-pass dichroic mirror and collected simultaneously through 100 μm pinholes and a 531 ± 20 nm bandpass filter (calcein channel) and a 630 ± 32 nm bandpass filter (propidium iodide channel) onto a low noise avalanche photodiode.

Photodynamic therapy was activated using a mercury arc lamp with a 692 ± 20 nm excitation filter, using neutral density filters to adjust the total incident power to 50 mW/cm^2.

■ ASSOCIATED CONTENT

Supporting Information

The Supporting Information is available free of charge on the ACS Publications website at DOI: 10.1021/acsabm.8b00315.

Figures of k-value determination for measured materials, translational diffusion constant "D" determination as a function of magnetic signal decay with increasing magnetic field strength "b", and uranyl acetate stained 8PEGA TEM (PDF)

■ AUTHOR INFORMATION

Corresponding Author

*Tel.: 734-764-7541. Fax: 734-936-2778. E-mail: kopelman@umich.edu.

ORCID

Thomas Hopkins: 0000-0002-5613-3449

Raoul Kopelman: 0000-0002-7770-8272

Author Contributions

§T.H. and S.D.S. contributed equally.

Notes

The authors declare no competing financial interest.

■ ACKNOWLEDGMENTS

We acknowledge support from the US National Institutes Of Health, NIH grant R01CA186769 (RK). We also acknowledge the NSF MRI-ID grant DBI-0959823 (Nils G. Walter PI) for seeding the Single Molecule Analysis in Real-Time (SMART) Center, which enabled the microscopy experiments, and the University of Michigan Microscopy and Image Analysis Laboratory for gathering TEMs.

■ REFERENCES

(1) Dougherty, T. J.; Gomer, C. J. Introduction. *Lasers Surg. Med.* **2011**, *43*, 541.

(2) Bernstein, Z. P.; Dougherty, T.; Gollnick, S.; Schwartz, S.; Mahajan, S.; Kepner, J.; Sumlin, A.; Stewart, C.; Wallace, P.; Walder, H.; Poiesz, B. Photopheresis in HIV-1 Infected Patients Utilizing Benzoporphyrin Derivative Verteporfin/BPD-MA and Light. *Curr. HIV Res.* **2007**, *6*, 152−163.

(3) Harrell, J.; Kopelman, R. Biocompatible Probes Measure Intracellular Activity. *Biophotonics Int.* **2000**, *7*, 22−24.

DOI: 10.1021/acsabm.8b00315
ACS Appl. Bio Mater. 2018, 1, 1094−1101

(4) Gupta, A.; Wang, S.; Pera, P.; Rao, K. V. R.; Patel, N.; Ohulchanskyy, T. Y.; Missert, J.; Morgan, J.; Koo-Lee, Y.; Kopelman, R.; Pandey, R. K. Multifunctional Nanoplatforms for Fluorescence Imaging and Photodynamic Therapy Developed by Post-loading Photosensitizer and Fluorophore to Polyacrylamide Nanoparticles. *Nanomedicine* **2012**, *8*, 941−950.
(5) Xu, H.; Buck, S. M.; Kopelman, R.; Philbert, M. A.; Brasuel, M.; Ross, B. D.; Rehemtulla, A. Photo-Excitation Based Nano-Explorers: Chemical Analysis Inside Live Cells and Photodynamic Therapy. *Isr. J. Chem.* **2004**, *44*, 317−337.
(6) Kopelman, R.; Lee-Koo, Y.; Philbert, M.; Moffat, B. A.; Reddy, R.; McConville, P.; Hall, D. E.; Chenevert, T. L.; Bhojani, M. S.; Buck, S. M.; Rehemtulla, A.; Ross, D. B. Multifunctional Nanoparticle Platforms for In Vivo MRI Enhancement and Photodynamic Therapy of a Rat Brain Cancer. *J. Magn. Magn. Mater.* **2005**, *293*, 404−410.
(7) Pandey, R. K.; Goswami, L. N.; Chen, Y.; Gryshuk, A.; Missert, J. R.; Oseroff, A.; Dougherty, T. J. Nature: A Rich Source for Developing Multifunctional Agents. Tumor-Imaging and Photodynamic Therapy. *Lasers Surg. Med.* **2006**, *38*, 445−467.
(8) Koo, Y. E.; Reddy, G. R.; Bhojani, M.; Schneider, R.; Philbert, M. A.; Rehemtulla, A.; Ross, B. D.; Kopelman, R. Brain Cancer Diagnosis and Therapy with Nanoplatforms. *Adv. Drug Delivery Rev.* **2006**, *58*, 1556−1577.
(9) Reddy, G. R.; Bhojani, M. S.; McConville, P.; Moody, J.; Moffat, B. A.; Hall, D. E.; Kim, G.; Koo, Y. E.; Wooliscroft, M. J.; Sugai, J. V.; Johnson, T. D.; Philbert, M. A.; Kopelman, R.; Rehemtulla, A.; Ross, B. D. Vascular Targeted Nanoparticles for Imaging and Treatment of Brain Tumors. *Clin. Cancer Res.* **2006**, *12*, 6677−6686.
(10) Baba, K.; Pudavar, H. E.; Roy, I.; Ohulchanskyy, T. Y.; Chen, Y.; Pandey, R.; Prasad, P. N. A New Method for Delivering a Hydrophobic Drug for Photodynamic Therapy Using Pure Nanocrystal Form of the Drug. *Mol. Pharmaceutics* **2007**, *4*, 289−297.
(11) Moreno, M. J.; Monson, E.; Reddy, R. G.; Rehemtulla, A.; Ross, B. D.; Philbert, M.; Schneider, R. J.; Kopelman, R. Production of Singlet Oxygen by $Ru(dpp)SO_3)_2)_3$ Incoproated in Polyacrylamide PEBBLES. *Sens. Actuators, B* **2003**, *90*, 82−89.
(12) Roy, I.; Ohulchanskyy, T. Y.; Pudavar, H. E.; Bergey, E. J.; Oseroff, A. R.; Morgan, J.; Dougherty, T. J.; Prasad, P. N. Ceramic-Based Nanoparticles Entrapping Water-Insoluble Photo-Sensitizing Anticancer Drugs: A Novel Drug-Carrier System for Therapy. *J. Am. Chem. Soc.* **2003**, *125*, 7860−7865.
(13) Avula, U. M.; Yoon, H. K.; Lee, C. H.; Kaur, K.; Ramirez, R. J.; Takemoto, Y.; Ennis, S. R.; Morady, F.; Herron, T.; Berenfeld, O.; Kopelman, R.; Kalifa, J. Cell-selective Arrhythmia Ablation for Photomodulation of Heart Rhythm. *Sci. Transl. Med.* **2015**, *7*, 311ra172.
(14) Karamchand, L.; Kim, G.; Wang, S.; Hah, H. J.; Ray, A.; Jiddou, R.; Lee, Y.E.k.; Philbert, M. A.; Kopelman, R. Modulation of Hydrogel Nanoparticle Intracellular Trafficking by Multivalent Surface Engineering with Tumor Targeting Peptide. *Nanoscale* **2013**, *5*, 10327.
(15) Watanabe, T.; Tsuge, H.; Imagawa, T.; Kise, D.; Hirano, K.; Beppu, M.; Takahashi, A.; Yamaguchi, K.; Fujiki, H.; Suganuma, M. Nucleolin as Cell Surface Receptor for Tumor Necrosis Factor-α Inducing Protein: A Carcinogenic Factor of *Helicobacter Pylori*. *J. Cancer Res. Clin. Oncol.* **2010**, *136*, 911−921.
(16) Hopkins, T.; Ukani, R.; Kopelman, R. Intracellular Photodynamic Activity of Chlorin e6 Containing Nanoparticles. *Int. J. Nanomed. Nanosurg.* **2016**, *3*, 119.
(17) Qin, M.; Hah, H. J.; Kim, G.; Nie, G.; Lee, Y. E.; Kopelman, R. Methylene Blue Covalently Loaded Polyacrylamide Nanoparticles for Enhanced Tumor-Targeted Photodynamic Therapy. *Photochem. Photobiol. Sci.* **2011**, *10*, 832−841.
(18) Hah, H. J.; Kim, G.; Lee, Y. E.; Orringer, D. A.; Sagher, O.; Philbert, M. A.; Kopelman, R. Methylene Blue-Conjugated Hydrogel Nanoparticles and Tumor-Cell Targeted Photodynamic Therapy. *Macromol. Biosci.* **2011**, *11*, 90−99.
(19) Lechner, M. D.; Machtle, W. Characterization of Nanoparticles. *Macromol. Symp.* **1999**, *145*, 1−7.
(20) Salmaso, S.; Caliceti, P. Stealth Properties to Improve Therapeutic Efficacy of Drug Nanocarriers. *J. Drug Delivery* **2013**, *2013*, 1.
(21) Nie, G.; Hah, H. J.; Lee, Y. E.; Qin, M.; Ratani, T. S.; Fotiadis, P.; Miller, A.; Kochi, A.; Gao, D.; Chen, T.; Orringer, D. A.; Sagher, O.; Philbert, M. A.; Kopelman, R. Hydrogel Nanoparticles with Covalently Linked Coomassie Blue for Brain Tumor Delineation Visible to the Surgeon. *Small* **2012**, *8*, 884−891.
(22) Henke, E.; Perk, J.; Vider, J.; Candia, P.; Chin, Y.; Solit, D. B.; Ponomarev, V.; Cartegni, L.; Manova, K.; Rosen, N.; Benezra, R. Peptide-Conjugated Antisense Oligonucleotides for Targeted Inhibition of a Transcriptional Regulator *In Vivo*. *Nat. Biotechnol.* **2008**, *26*, 91−100.
(23) Winer, I.; Wang, S.; Lee, Y. E.; Fan, W.; Gong, Y.; Burgos-Ojeda, D.; Spahlinger, G.; Kopelman, R.; Buckanovich, R. J. F3-Targeted Cisplatin-Hydrogel Nanoparticles as an Effective Therapeutic That Targets Both Murine and Huamn Ovarian Tumor Endothelial Cell *In Vivo*. *Cancer Res.* **2010**, *70*, 8674−8683.
(24) Aluigi, A.; Sotgiu, G.; Ferroni, C.; Duchi, S.; Lucarelli, E.; Martini, C.; Posati, T.; Guerrini, A.; Ballestri, M.; Corticelli, F.; Varchi, G. Chlorin e6 Keratin Nanoparticles for Photodynamic Anticancer Therapy. *RSC Adv.* **2016**, *6*, 33910−33918.
(25) Bharathiraja, S.; Moorthy, M. S.; Manivasagan, P.; Seo, H.; Lee, K. D.; Oh, J. Chlorin e6 Conjugated Silica Nanoparticles for Targeted and Effective Photodynamic Therapy. *Photodiagn. Photodyn. Ther.* **2017**, *19*, 212−220.
(26) Bharathiraja, S.; Manivasagan, P.; Moorthy, M. S.; Bui, N. Q.; Lee, K. D.; Oh, J. Chlorin e6 Conjugated Copper Sulfide Nanoparticles for Photodynamic Combined Photothermal Therapy. *Photodiagn. Photodyn. Ther.* **2017**, *19*, 128−134.
(27) Hou, W.; Xia, F.; Alves, C. S.; Qian, X.; Yang, Y.; Cui, D. MMP2-Targeting and Redox-Responsive PEGylated Chorin e6 Nanoparticles for Cancer Near-Infrared Imaging and Photodynamic Therapy. *ACS Appl. Mater. Interfaces* **2016**, *8*, 1447−1457.
(28) Zhang, D.; Wu, M.; Zeng, Y.; Wu, L.; Wang, Q.; Han, X.; Liu, X.; Liu, J. Chlorin e6 Conjugated Poly(dopamine) Nanospheres as PDT/PTT Dual-Modal Therapeutic Agents for Enhanced Cancer Therapy. *ACS Appl. Mater. Interfaces* **2015**, *7*, 8176−8187.
(29) Pezzella, F.; Gatter, K.C. Evidence Showing That Tumors Can Grow Without Angiogenesis and Can Switch Between Angiogenic and Nonangiogenic Phenotypes. *J. Natl. Cancer Inst.* **2016**, *108*, 32.
(30) Alvares, R. D. A.; Lau, J. Y. C.; Macdonald, P. M.; Cunningham, C. H.; Prosser, R. S. Direct Quantitative ^{13}C-Filtered ^{1}H Magnetic Resonance Imaging of PEGylated Biomacromolecules In Vivo. *Magn. Reson. Med.* **2017**, *77*, 1553−1561.
(31) Bieze, T. W. N.; van der Maarel, J. R. C.; Eisenbach, C. D.; Leyte, J. C. Polymer Dynamics in Aqueous Poly(ethylene oxide) Solutions. *Macromolecules* **1994**, *27*, 1355−1366.
(32) Stejskal, E. O.; Tanner, J. E. Spin Diffusion Measurements: Spin Echoes in the Presence of a Time-Dependent Field Gradient. *J. Chem. Phys.* **1965**, *42*, 288−292.

DOI: 10.1021/acsabm.8b00315
ACS Appl. Bio Mater. 2018, 1, 1094−1101